EUROPEAN ORGANISATION FOR NUCLEAR RESEARCH

CERN-PPE/94-171
3 November 1994

A Test of $\mathcal{CP}$-Invariance in $Z^0 \longrightarrow \tau^+\tau^-$ Using Optimal Observables

The OPAL Collaboration

Abstract

Using 27 490 $Z^0 \to \tau^+\tau^-$ decays, accumulated in 1991, 1992 and 1993 with the OPAL detector at LEP, a direct test of $\mathcal{CP}$-invariance in the neutral current reaction $e^+e^- \longrightarrow \tau^+\tau^-$ is performed by measuring $\mathcal{CP}$-odd observables which are proportional to the weak dipole moment of the τ-lepton. A new method based on optimal $\mathcal{CP}$-odd observables constructed from the τ flight and spin directions is employed. More sensitive measurements of the real and, for the first time, the imaginary part of the weak dipole moment with highest possible signal to noise ratio are obtained. No evidence for a non-zero expectation value of the considered observables and hence for $\mathcal{CP}$-violation is observed. An upper limit on the weak dipole moment of $|\,\mathrm{Re}(d_\tau^w)\,| < 7.8 \times 10^{-18}\ e \cdot \mathrm{cm}$ and $|\,\mathrm{Im}(d_\tau^w)\,| < 4.5 \times 10^{-17}\ e \cdot \mathrm{cm}$ with 95% confidence level is obtained.

(to be submitted to Zeitschrift für Physik C)

The OPAL Collaboration

R. Akers[16], G. Alexander[23], J. Allison[16], K. Ametewee[25], K.J. Anderson[9], S. Arcelli[2], S. Asai[24], A. Astbury[28], D. Axen[29], G. Azuelos[18,a], A.H. Ball[17], E. Barberio[26], R.J. Barlow[16], R. Bartoldus[3], J.R. Batley[5], G. Beaudoin[18], A. Beck[23], G.A. Beck[13], C. Beeston[16], T. Behnke[27], K.W. Bell[20], G. Bella[23], S. Bentvelsen[8], P. Berlich[10], S. Bethke[32], O. Biebel[32], I.J. Bloodworth[1], P. Bock[11], H.M. Bosch[11], M. Boutemeur[18], S. Braibant[12], P. Bright-Thomas[25], R.M. Brown[20], A. Buijs[8], H.J. Burckhart[8], R. Bürgin[10], C. Burgard[27], N. Capdevielle[18], P. Capiluppi[2], R.K. Carnegie[6], A.A. Carter[13], J.R. Carter[5], C.Y. Chang[17], C. Charlesworth[6], D.G. Charlton[8], S.L. Chu[4], P.E.L. Clarke[15], J.C. Clayton[1], S.G. Clowes[16], I. Cohen[23], J.E. Conboy[15], M. Cuffiani[2], S. Dado[22], C. Dallapiccola[17], G.M. Dallavalle[2], C. Darling[31], S. De Jong[12], L.A. del Pozo[8], H. Deng[17], M. Dittmar[4], M.S. Dixit[7], E. do Couto e Silva[12], J.E. Duboscq[8], E. Duchovni[26], G. Duckeck[8], I.P. Duerdoth[16], U.C. Dunwoody[5], P.A. Elcombe[5], P.G. Estabrooks[6], E. Etzion[23], H.G. Evans[9], F. Fabbri[2], B. Fabbro[21], M. Fanti[2], P. Fath[11], M. Fierro[2], M. Fincke-Keeler[28], H.M. Fischer[3], P. Fischer[3], R. Folman[26], D.G. Fong[17], M. Foucher[17], H. Fukui[24], A. Fürtjes[8], P. Gagnon[6], A. Gaidot[21], J.W. Gary[4], J. Gascon[18], N.I. Geddes[20], C. Geich-Gimbel[3], S.W. Gensler[9], F.X. Gentit[21], T. Geralis[20], G. Giacomelli[2], P. Giacomelli[4], R. Giacomelli[2], V. Gibson[5], W.R. Gibson[13], J.D. Gillies[20], J. Goldberg[22], D.M. Gingrich[30,a], M.J. Goodrick[5], W. Gorn[4], C. Grandi[2], E. Gross[26], J. Hagemann[27], G.G. Hanson[12], M. Hansroul[8], C.K. Hargrove[7], P.A. Hart[9], M. Hauschild[8], C.M. Hawkes[8], E. Heflin[4], R.J. Hemingway[6], G. Herten[10], R.D. Heuer[8], J.C. Hill[5], S.J. Hillier[8], T. Hilse[10], P.R. Hobson[25], D. Hochman[26], A. Höcker[3], R.J. Homer[1], A.K. Honma[28,a], R. Howard[29], R.E. Hughes-Jones[16], P. Igo-Kemenes[11], D.C. Imrie[25], A. Jawahery[17], P.W. Jeffreys[20], H. Jeremie[18], M. Jimack[1], M. Jones[6], R.W.L. Jones[8], P. Jovanovic[1], C. Jui[4], D. Karlen[6], J. Kanzaki[24], K. Kawagoe[24], T. Kawamoto[24], R.K. Keeler[28], R.G. Kellogg[17], B.W. Kennedy[20], B. King[8], J. King[13], J. Kirk[29], S. Kluth[5], T. Kobayashi[24], M. Kobel[10], D.S. Koetke[6], T.P. Kokott[3], S. Komamiya[24], R. Kowalewski[8], T. Kress[11], P. Krieger[6], J. von Krogh[11], P. Kyberd[13], G.D. Lafferty[16], H. Lafoux[8], R. Lahmann[17], W.P. Lai[19], J. Lauber[8], J.G. Layter[4], P. Leblanc[18], P. Le Du[21], A.M. Lee[31], E. Lefebvre[18], D. Lellouch[26], C. Leroy[18], J. Letts[4], L. Levinson[26], Z. Li[12], F. Liu[29], S.L. Lloyd[13], F.K. Loebinger[16], G.D. Long[17], B. Lorazo[18], M.J. Losty[7], X.C. Lou[8], J. Ludwig[10], A. Luig[10], M. Mannelli[8], S. Marcellini[2], C. Markus[3], A.J. Martin[13], J.P. Martin[18], T. Mashimo[24], W. Matthews[25], P. Mättig[3], U. Maur[3], J. McKenna[29], T.J. McMahon[1], A.I. McNab[13], F. Meijers[8], F.S. Merritt[9], H. Mes[7], A. Michelini[8], R.P. Middleton[20], G. Mikenberg[26], D.J. Miller[15], R. Mir[26], W. Mohr[10], A. Montanari[2], T. Mori[24], M. Morii[24], U. Müller[3], B. Nellen[3], B. Nijjhar[16], S.W. O'Neale[1], F.G. Oakham[7], F. Odorici[2], H.O. Ogren[12], C.J. Oram[28,a], M.J. Oreglia[9], S. Orito[24], J.P. Pansart[21], G.N. Patrick[20], M.J. Pearce[1], P.D. Phillips[16], J.E. Pilcher[9], J. Pinfold[30], D. Pitman[28], D.E. Plane[8], P. Poffenberger[28], B. Poli[2], A. Posthaus[3], T.W. Pritchard[13], H. Przysiezniak[18], M.W. Redmond[8], D.L. Rees[8], D. Rigby[1], M. Rison[5], S.A. Robins[13], D. Robinson[5], N. Rodning[30], J.M. Roney[28], E. Ros[8], A.M. Rossi[2], M. Rosvick[28], P. Routenburg[30], Y. Rozen[8], K. Runge[10], O. Runolfsson[8], D.R. Rust[12], M. Sasaki[24], C. Sbarra[2], A.D. Schaile[8], O. Schaile[10], F. Scharf[3], P. Scharff-Hansen[8], P. Schenk[4], B. Schmitt[3], M. Schröder[12], H.C. Schultz-Coulon[10], P. Schütz[3], M. Schulz[8], C. Schwick[27], J. Schwiening[3], W.G. Scott[20], M. Settles[12], T.G. Shears[5], B.C. Shen[4], C.H. Shepherd-Themistocleous[7], P. Sherwood[15], G.P. Siroli[2], A. Skillman[16], A. Skuja[17], A.M. Smith[8], T.J. Smith[28], G.A. Snow[17], R. Sobie[28],

S. Söldner-Rembold[10], R.W. Springer[30], M. Sproston[20], A. Stahl[3], M. Starks[12], C. Stegmann[10], K. Stephens[16], J. Steuerer[28], B. Stockhausen[3], D. Strom[19], P. Szymanski[20], R. Tafirout[18], H. Takeda[24], T. Takeshita[24], P. Taras[18], S. Tarem[26], M. Tecchio[9], P. Teixeira-Dias[11], N. Tesch[3], M.A. Thomson[15], O. Tousignant[18], S. Towers[6], M. Tscheulin[10], T. Tsukamoto[24], A. Turcot[9], M.F. Turner-Watson[8], P. Utzat[11], R. Van Kooten[12], G. Vasseur[21], P. Vikas[18], M. Vincter[28], A. Wagner[27], D.L. Wagner[9], C.P. Ward[5], D.R. Ward[5], J.J. Ward[15], P.M. Watkins[1], A.T. Watson[1], N.K. Watson[7], P. Weber[6], P.S. Wells[8], N. Wermes[3], B. Wilkens[10], G.W. Wilson[27], J.A. Wilson[1], V-H. Winterer[10], T. Wlodek[26], G. Wolf[26], S. Wotton[11], T.R. Wyatt[16], A. Yeaman[13], G. Yekutieli[26], M. Yurko[18], V. Zacek[18], W. Zeuner[8], G.T. Zorn[17].

[1]School of Physics and Space Research, University of Birmingham, Birmingham B15 2TT, UK
[2]Dipartimento di Fisica dell' Università di Bologna and INFN, I-40126 Bologna, Italy
[3]Physikalisches Institut, Universität Bonn, D-53115 Bonn, Germany
[4]Department of Physics, University of California, Riverside CA 92521, USA
[5]Cavendish Laboratory, Cambridge CB3 0HE, UK
[6]Carleton University, Department of Physics, Colonel By Drive, Ottawa, Ontario K1S 5B6, Canada
[7]Centre for Research in Particle Physics, Carleton University, Ottawa, Ontario K1S 5B6, Canada
[8]CERN, European Organisation for Particle Physics, CH-1211 Geneva 23, Switzerland
[9]Enrico Fermi Institute and Department of Physics, University of Chicago, Chicago IL 60637, USA
[10]Fakultät für Physik, Albert Ludwigs Universität, D-79104 Freiburg, Germany
[11]Physikalisches Institut, Universität Heidelberg, D-69120 Heidelberg, Germany
[12]Indiana University, Department of Physics, Swain Hall West 117, Bloomington IN 47405, USA
[13]Queen Mary and Westfield College, University of London, London E1 4NS, UK
[15]University College London, London WC1E 6BT, UK
[16]Department of Physics, Schuster Laboratory, The University, Manchester M13 9PL, UK
[17]Department of Physics, University of Maryland, College Park, MD 20742, USA
[18]Laboratoire de Physique Nucléaire, Université de Montréal, Montréal, Quebec H3C 3J7, Canada
[19]University of Oregon, Department of Physics, Eugene OR 97403, USA
[20]Rutherford Appleton Laboratory, Chilton, Didcot, Oxfordshire OX11 0QX, UK
[21]CEA, DAPNIA/SPP, CE-Saclay, F-91191 Gif-sur-Yvette, France
[22]Department of Physics, Technion-Israel Institute of Technology, Haifa 32000, Israel
[23]Department of Physics and Astronomy, Tel Aviv University, Tel Aviv 69978, Israel
[24]International Centre for Elementary Particle Physics and Department of Physics, University of Tokyo, Tokyo 113, and Kobe University, Kobe 657, Japan
[25]Brunel University, Uxbridge, Middlesex UB8 3PH, UK
[26]Particle Physics Department, Weizmann Institute of Science, Rehovot 76100, Israel
[27]Universität Hamburg/DESY, II Institut für Experimental Physik, Notkestrasse 85, D-22607 Hamburg, Germany

[28]University of Victoria, Department of Physics, P O Box 3055, Victoria BC V8W 3P6, Canada
[29]University of British Columbia, Department of Physics, Vancouver BC V6T 1Z1, Canada
[30]University of Alberta, Department of Physics, Edmonton AB T6G 2J1, Canada
[31]Duke University, Dept of Physics, Durham, NC 27708-0305, USA
[32]Technische Hochschule Aachen, III Physikalisches Institut, Sommerfeldstrasse 26-28, D-52056 Aachen, Germany

[a]Also at TRIUMF, Vancouver, Canada V6T 2A3

1 Introduction

In the Standard Model, $\mathcal{CP}$-violation has its origin in the charged current couplings among quarks and is described by a phase in the CKM-matrix [1]. Violation of $\mathcal{CP}$-symmetry has so far not been observed in neutral current reactions, and the Standard Model does not predict any measurable effects there [2].

In neutral current processes $\mathcal{CP}$-violation can be introduced if the participating particles possess electric or weak dipole moments. For two reasons it is advantageous to use the $\mathrm{Z}^0 \to \tau^+\tau^-$ decay in the search for $\mathcal{CP}$-violation. First, the $\mathcal{CP}$-violating dipole moment is related to the spin of the outgoing fermion. Due to its short lifetime the τ-lepton decays inside the detector and transfers information about its spin to the energies and momenta of its decay products. Second, $\mathcal{CP}$-violating models exist [2, 3] in which the magnitude of the lepton dipole moment depends on the mass of the fermion to the third power, thus favoring processes with heavy fermions.

$\mathcal{CP}$-violation in $\mathrm{Z}^0 \to \tau^+\tau^-$ decays can be studied by measuring $\mathcal{CP}$-odd observables. If $\mathcal{CP}$-invariance holds, the mean value of these observables must be zero. Any observation of a non-zero expectation value of $\mathcal{CP}$-odd observables would indicate physics beyond the Standard Model.

Taking into account operators with mass dimension $d \leq 6$, the $\mathcal{CP}$-violating effective Lagrangian of the $\tau^+\tau^-$ production vertex is given by [2]

$$\mathcal{L}_{\mathcal{CP}} \;=\; -\frac{i}{2}\bar{\tau}\sigma^{\mu\nu}\gamma_5\tau\,\left(\,d^e_\tau(q^2)F_{\mu\nu} \;+\; d^w_\tau(q^2)Z_{\mu\nu}\,\right) \tag{1}$$

where $F_{\mu\nu}$ and $Z_{\mu\nu}$ are the electromagnetic and weak field tensors. The electric and weak dipole form factors are denoted by $d^e_\tau(q^2)$ and $d^w_\tau(q^2)$, respectively. They determine the strength of the $\mathcal{CP}$-violating amplitude and may have a real as well as an imaginary part. At LEP the momentum transfer q is given by $q^2 \cong m^2_{\mathrm{Z}}$ and $d^w_\tau(m^2_{\mathrm{Z}})$, which dominates at this q^2, is now called the weak dipole moment. The $\mathcal{CP}$-violating transition amplitude $T_{\mathcal{CP}}$, with coupling strength d^w_τ, occurs in addition to the Standard Model amplitude T_{SM}. For large d^w_τ the interaction $\mathcal{L}_{\mathcal{CP}}$ gives rise to a non-negligible $\mathcal{CP}$-even contribution, $|T_{\mathcal{CP}}|^2$, to the cross section $\mathrm{d}\sigma \propto |T_{\mathrm{SM}} + T_{\mathcal{CP}}|^2$ and the partial width $\Gamma(\mathrm{Z}^0 \to \tau^+\tau^-)$. In principle a measurement of the partial width for $\mathrm{Z}^0 \to \tau^+\tau^-$ does not constitute a test of $\mathcal{CP}$-invariance. However, it can be used to determine d^w_τ under the assumption that no interaction outside the Standard Model other than $\mathcal{L}_{\mathcal{CP}}$ contributes to the width. With this method an upper limit on d^w_τ from $\Gamma(\mathrm{Z}^0 \to \tau^+\tau^-)$ [4] of $2.2 \times 10^{-17}\, e\cdot$cm at the 95% c.l. can be derived. The $\mathcal{CP}$-odd interference term, in contrast, gives rise to $\mathcal{CP}$-violating effects.

2 $\mathcal{CP}$-odd Observables

$\mathcal{CP}$-odd observables, $\mathcal{O}$, have various transformation properties under time reversal. $\mathcal{CP}$-odd and $\mathcal{T}$-odd observables $\mathcal{O}^{\mathcal{T}^-}$ transform $\mathcal{CPT}$-even. Their mean values are proportional to $\mathrm{Re}(d^w_\tau)$. $\mathcal{CP}$-odd and $\mathcal{T}$-even observables $\mathcal{O}^{\mathcal{T}^+}$ transform $\mathcal{CPT}$-odd. Given $\mathcal{CPT}$-invariance, which is assumed throughout this paper, a non-zero mean value would be proportional to $\mathrm{Im}(d^w_\tau)$. This requires absorptive parts in a $\mathcal{CP}$-non-conserving interaction.

Let us consider the reaction

$$e^+e^- \longrightarrow \tau^+(k^+)\,\tau^-(k^-) \longrightarrow A^+(p_A)\,B^-(p_B)\,\nu_\tau\bar{\nu}_\tau \tag{2}$$

where A and B are hadronic or leptonic final states emerging from τ^+ and τ^- decays, respectively; and $k^\pm$ and $p_{A/B}$ are their respective four momenta. In the presence of a weak dipole moment the following relations hold:

$$\begin{aligned} \langle \mathcal{O}^{\mathcal{T}^-} \rangle_{AB} &= \frac{m_Z}{e} c_{AB}\,\mathrm{Re}(d_\tau^w) \\ \langle \mathcal{O}^{\mathcal{T}^+} \rangle_{AB} &= \frac{m_Z}{e} f_{AB}\,\mathrm{Im}(d_\tau^w)\ , \end{aligned} \tag{3}$$

i.e., the mean values of the observables $\mathcal{O}^{\mathcal{T}^\pm}$ are directly proportional to the weak dipole moment. The dimensionless proportionality constants c_{AB} and f_{AB} are called *sensitivities* and depend on the respective τ decay modes A, B. (See section 6.) Many observables can be constructed which transform odd under $\mathcal{CP}$, such as $T_{ij} = (\mathbf{p}_A - \mathbf{p_B})_i(\mathbf{p}_A \times \mathbf{p}_B)_j + (i \leftrightarrow j)$, which was used in previous analyses [5, 6]. The optimal choice is obviously the one which maximizes the signal-to-noise ratio

$$R^\pm = \sqrt{\frac{\langle \mathcal{O}^{\mathcal{T}^\pm} \rangle^2}{\langle (\mathcal{O}^{\mathcal{T}^\pm})^2 \rangle - \langle \mathcal{O}^{\mathcal{T}^\pm} \rangle^2}} \quad . \tag{4}$$

This condition is met by observables of the form [7]

$$\mathcal{O}^{\mathcal{T}^\pm} = \frac{\mathrm{d}\sigma^{\mathcal{T}^\pm}_{\mathcal{CP}}}{\mathrm{d}\sigma_{\mathrm{SM}}}\ . \tag{5}$$

Here $\mathrm{d}\sigma^{\mathcal{T}^\pm}_{\mathcal{CP}}$ are the terms in the differential cross section for $e^+e^- \to \tau^+\tau^-$ which are $\mathcal{CP}$-odd and $\mathcal{T}$-odd ($\mathcal{T}^-$) or $\mathcal{CP}$-odd and $\mathcal{T}$-even ($\mathcal{T}^+$), respectively, and $\mathrm{d}\sigma_{\mathrm{SM}}$ is the differential cross section of the Standard Model. Neglecting all terms of the τ pair spin density matrix [8], which are proportional to the small neutral vector coupling constants to leptons g_V ($g_V/g_A = 0.075 \pm 0.003$ [4]), the leading terms of the differential cross sections in equation (5) are given by

$$\mathrm{d}\sigma^{\mathcal{T}^+}_{\mathcal{CP}} \propto M^{\mathrm{Re}}_{\mathcal{CP}} = (\hat{\mathbf{k}}\cdot\hat{\mathbf{q}}_e)\left(\hat{\mathbf{k}} \times (\mathbf{S}^+ - \mathbf{S}^-)\right)\cdot\hat{\mathbf{q}}_e \tag{6}$$

$$\mathrm{d}\sigma^{\mathcal{T}^-}_{\mathcal{CP}} \propto M^{\mathrm{Im}}_{\mathcal{CP}} = (\hat{\mathbf{k}}\cdot\hat{\mathbf{q}}_e)\left[(\hat{\mathbf{k}}\cdot\mathbf{S}^+)(\hat{\mathbf{q}}_e\cdot\mathbf{S}^-) - (\hat{\mathbf{k}}\cdot\mathbf{S}^-)(\hat{\mathbf{q}}_e\cdot\mathbf{S}^+)\right] \tag{7}$$

$$\begin{aligned} \mathrm{d}\sigma_{\mathrm{SM}} \propto M_{SM} = 1 &+ (\hat{\mathbf{k}}\cdot\hat{\mathbf{q}}_e)^2 + \mathbf{S}^+\cdot\mathbf{S}^-(1 - (\hat{\mathbf{k}}\cdot\hat{\mathbf{q}}_e)^2) - 2(\hat{\mathbf{q}}_e\cdot\mathbf{S}^+)(\hat{\mathbf{q}}_e\cdot\mathbf{S}^-) \\ &+ 2(\hat{\mathbf{k}}\cdot\hat{\mathbf{q}}_e)\left[(\hat{\mathbf{k}}\cdot\mathbf{S}^+)(\hat{\mathbf{q}}_e\cdot\mathbf{S}^-) + (\hat{\mathbf{k}}\cdot\mathbf{S}^-)(\hat{\mathbf{q}}_e\cdot\mathbf{S}^+)\right]. \end{aligned} \tag{8}$$

Here $\hat{\mathbf{q}}_e$ is the direction of the electron beam, $\hat{\mathbf{k}}$ is the flight direction of the positive τ and the $\mathbf{S}^\pm$ are the spin vectors of the $\tau^\pm$ leptons in their respective rest systems[1]. The observable used in this analysis then becomes

$$\mathcal{O}^{\mathcal{T}^\pm} = \frac{M^{\mathrm{Re/Im}}_{\mathcal{CP}}}{M_{\mathrm{SM}}}\ . \tag{9}$$

[1] Throughout this paper three-dimensional vectors are printed in bold letters

Neither the τ spin nor the τ flight direction can be measured directly. Their reconstruction is described in the appendix. Figure 1 shows the distributions of this $\mathcal{CP}$-odd observable (9) in the decay mode $\tau^+\tau^- \to \pi^+\pi^-\,\nu_\tau\bar{\nu}_\tau$ generated by Monte Carlo simulation. For non-zero dipole moments the expectation values of the respective observables are no longer zero.

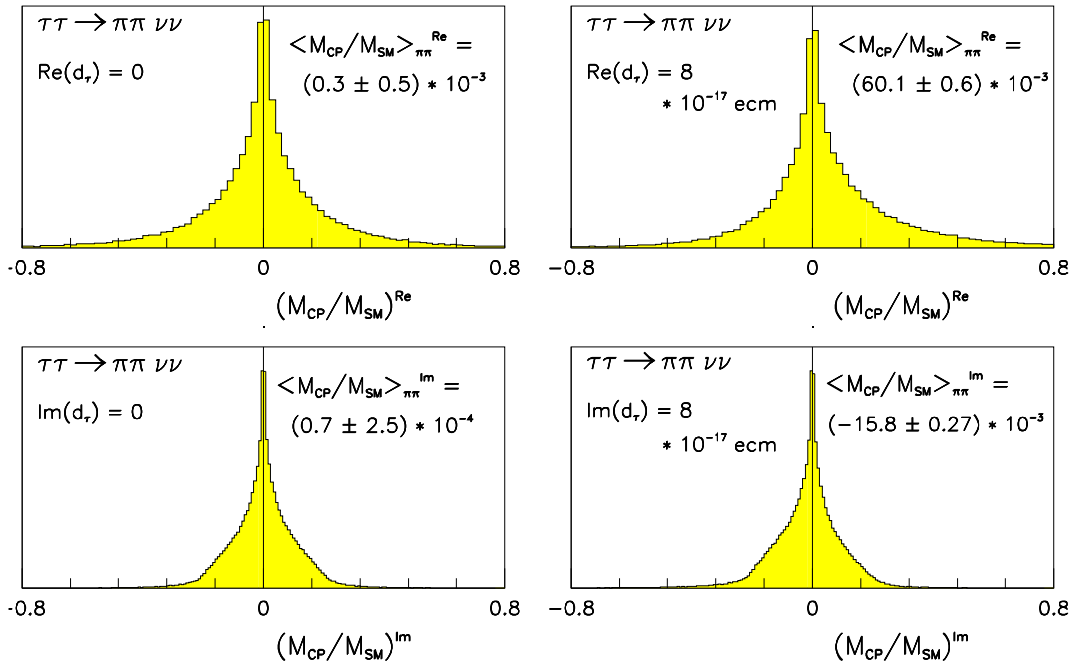

Figure 1: $M_{\mathcal{CP}}/M_{\rm SM}$ in the $\tau^+\tau^- \to \pi^+\pi^-\,\nu\bar{\nu}$ decay for zero d_τ^w (left side) and $\mathrm{Re}(d_\tau^w)$=$\mathrm{Im}(d_\tau^w) = 8\times10^{-17}\,e$·cm (right side). The plots show 200 000 simulated events.

3 The OPAL Detector

OPAL is an experiment collecting data at the LEP $\mathrm{e^+e^-}$ storage ring, which operates at c.m. energies near the $\mathrm{Z^0}$ peak. Since a detailed description of the OPAL detector is given in [9, 10], we describe briefly the most important elements involved in this analysis.

The central tracking chambers at OPAL are contained in a 4 bar pressure vessel and immersed in a 0.435 T axial magnetic field. Moving from small to large radius, the tracking system consists of a precision vertex drift chamber with 12 axial wires and 6 small angle stereo wires extending in radius from about 10-21 cm, a large volume (4 m long, 3.7 m diameter) drift chamber (jet-chamber) with 159 layers of axial anode wires and z-chambers which provide up to six precise measurements of the z-coordinate of charged particles as they leave the tracking system. Before the 1991 run a silicon micro-vertex detector was installed with silicon planes at radii of 6.1 and 7.5 cm. The jet-chamber allows the full 159 measurements over the polar angle range $|\cos\theta| < 0.73$, while the z-chambers provide measurements to $|\cos\theta| < 0.72$. The jet-chamber also provides measurements of the specific energy loss of tracks in matter $(\mathrm{d}E/\mathrm{d}x)$.

Electromagnetic energy is measured by a detector composed of lead-glass blocks located outside the magnetic coil, divided into a barrel ($|\cos\theta| < 0.82$) and two endcaps ($0.81 <$

$|\cos\theta| < 0.98$). Each block subtends approximately 40×40 mrad^2. The depth of material to the back of the calorimeter is about 25 radiation lengths. The electromagnetic calorimeter has a time-of-flight detector and a preshower system (presampler) in front of it. The presampler consists of limited streamer tubes in the barrel region and thin multiwire chambers in the endcaps.

Outside the electromagnetic calorimeter, the OPAL detector is instrumented with a hadron calorimeter, constructed from alternating layers of iron slabs and limited streamer tubes. The total thickness of the material is typically eight interaction lengths. Outside the hadron calorimeter is the muon chamber system, composed of four layers of drift chambers for $|\cos\theta| < 0.68$ and four layers of limited streamer tubes for $0.60 < |\cos\theta| < 0.98$.

4 τ-Pair Selection

This analysis uses τ decay modes with one and three charged tracks. The data used for this analysis were recorded with the OPAL detector at LEP during 1991, 1992 and 1993. The integrated luminosity represents $69.1\,pb^{-1}$, distributed in energy around the Z^0 peak and corresponds to 87 600 produced $\tau^+\tau^-$ events.

The topology of $e^+e^- \to \tau^+\tau^-$ events is characterized by a pair of back-to-back, narrow jets with low particle multiplicity. These characteristics are exploited by dividing the event into jets whose tracks and clusters are assigned to cones of half-angle 35°. For the selection of τ-pairs we follow our standard selection criteria [11].

Three main background sources have to be considered. $Z^0 \to q\bar{q}$ events are removed by requiring at least two, but not more than six tracks which passed standard quality cuts and not more than ten clusters in the electromagnetic calorimeter. Background from two photon events is removed by cuts on the visible energy. In addition the minimal total transverse momentum has to be at least 2 GeV when the visible energy is below 18 GeV and we also demand an angle of acollinearity smaller than 15° between the jet axes. A less important type of background arises from cosmic rays. This is suppressed by requirements on the time-of-flight and by the location of the event vertex and the event topology. Details can be found in [11].

The remaining events are almost entirely lepton pairs: $e^+e^- \to e^+e^-$ and $e^+e^- \to \mu^+\mu^-$ events are removed by cuts on the energy deposited in the electromagnetic calorimeter, the momenta and signals in the muon chambers.

A total of 71 147 τ-pairs have been found. This corresponds to a detection efficiency of about 80%.

5 Selection of τ Decay Channels

To select the τ decay channels a maximum likelihood method (channel likelihood [12]) is employed, combining different information (variables) measured for an individual event. The likelihood algorithm is applied to an individual cone and assigns a specific τ decay channel to it. The following classifications for one-prong and three-prong decay modes are used.

For one-prong decays: $\tau \to e\nu_e\nu_\tau$,
$\tau \to \mu\nu_\mu\nu_\tau$,
$\tau \to \pi\nu_\tau$,
$\tau \to \rho\nu_\tau$,
$\tau \to a_1\nu_\tau$, with $a_1 \to \pi^\pm 2\pi^0$.

For three-prong decays: $\tau \to a_1\nu_\tau$, with $a_1 \to 3\pi^\pm$,
$\tau \to K^*\nu_\tau$,
$\tau \to 3\pi^\pm(\geq 1\pi^0)\,\nu_\tau$ and
one-prong decays accompanied by an electron-positron pair from a converted photon or a Dalitz decay.

In the likelihood procedure the detector has been subdivided into three different geometrical regions named barrel ($|\cos\theta| \leq 0.68$), overlap ($0.68 < |\cos\theta| \leq 0.76$), and endcaps ($0.76 < |\cos\theta| \leq 0.95$), where θ is the polar angle between track and beam axis. This is due to the $\cos\theta$ dependence of the misidentification probabilities and the sensitivities (see section 6).

5.1 The Detector Variables

The variables used to identify τ decays into one charged track (one-prong) are:

- The ratio of the energy deposited in the electromagnetic calorimeter over the momentum measured in the tracking chambers (E/p).
- Electromagnetic energy not assigned to the charged track ($E_{\rm ntrl}$).
- The minimum number of lead glass blocks containing at least 90 % of the cluster energy ($N_{\rm bl}$). The average value expected for electrons (about 2 blocks) is subtracted.
- The maximum angle between a presampler cluster and the charged track in the cone ($\Delta\Phi_{\rm max}$). (There is no coverage in the range $0.80 < |\cos\theta| < 0.82$.)
- The deviation of the measured energy loss in the jet chamber ($\mathrm{d}E/\mathrm{d}x$) from the energy loss expected from the charged particle of each decay channel.
- The number of hits within the three last planes of the hadron calorimeter and the muon chambers. ($N_{\rm hits}$).
- The number of hits per layer in the hadron calorimeter ($N_{\rm hits/layer}$).
- The matching of the track segment in the muon chambers with the charged track ($\log(\omega_{\mu-\rm ch.})$).

The following one-prong variables are shower shape variables based on a cluster algorithm, which helps to identify the $\tau \to \rho\nu_\tau \to \pi\pi^0\,\nu_\tau$ decay. They are only used in the barrel region.

- The invariant mass of the charged track with the reconstructed π^0, if any (M_ρ).
- The invariant mass of the two reconstructed photons, if any.
- The residual mass and energy in the electromagnetic calorimeter after subtracting the ρ.
- The angle of the pions in the ρ rest frame with respect to the ρ direction of flight.

The variables used to identify τ decays into three charged tracks (three-prong) are:

- The probability for each track to be an electron or a pion calculated from the dE/dx information is used to calculate the probability that all 3 tracks are pions compared to 1 pion plus 2 electrons from a conversion.
- The 3 tracks are fitted to a common vertex. The quality (χ^2) of the fit is used.
- The ratio of electromagnetic energy over charged momentum, both summed over the cone.
- The multiplicity measured in the presampler and not associated to a track.

The first two variables reduce the background from one-prongs plus conversion. The last two variables distinguish between the three–prong channels with and without neutral pions.

5.2 The Likelihood Identification Method

For the classification of τ decays into the various τ decay modes good tracks and clusters are selected, a $\tau^+\tau^-$ event is divided into two cones and the detector variables are calculated. The measured values of the considered variables are compared to properly normalized reference distributions taken from simulated events for all decay channels mentioned above. Assuming $N_{\rm var}$ variables and $N_{\rm par}$ decay channels, each variable i for τ decay channel j is distributed according to the (normalized) probability density function $f_i^j(x_i)$ given by a reference distribution taken from the Monte Carlo (KORALZ 3.8[13]/TAUOLA 1.5[14]) plus detector simulation [15, 16]. The probability for a particular configuration then is

$$p_i^j(x_i) \;=\; \frac{f_i^j(x_i)}{\sum_{j=1}^{N_{\rm par}} f_i^j(x_i)} \;. \tag{10}$$

The $p_i^j(x_i)$ are multiplied and normalized to obtain the likelihood function

$$\mathcal{L}^j(x) \;=\; \frac{\prod_{i=1}^{N_{\rm var}} p_i^j(x_i)}{\sum_{j=1}^{N_{\rm par}} \left(\prod_{i=1}^{N_{\rm var}} p_i^j(x_i)\right)} \;. \tag{11}$$

An event is assigned to the particular decay channel for which it has the maximum likelihood.

In tables 1 and 2 the efficiencies and the purities of the maximum likelihood selection for the respective τ decay modes are listed. They are calculated in the three different geometrical regions: barrel, overlap and endcap. The entries in table 1 are the probabilities for classifying the original decay channels in the left column as the final states given in the header lines. One notes that around 35% (barrel) of the ρ events are not identified as one of the considered τ decay products. The missing events are mostly detected in the a_1 1-prong channel.

It is important to study the uncertainties of the background in the various τ decay channels, especially the migration from other τ decay channels, because they dominate the systematic errors of the sensitivities. (See section 6.) These uncertainties are derived by modifying the Monte Carlo reference distributions within ranges obtained from test samples in the data. Only part of the detector components are used to identify τ decay channels. Then those samples can be used to check the distributions of the variables derived from the unused detector components. Two independent test samples, type 1 and type 2, were selected using information from:

Monte Carlo τ-decay channel	reconstruction efficiency (%) barrel				overlap				endcaps			
1 prong	e	μ	π	ρ	e	μ	π	ρ	e	μ	π	ρ
e	94.7	0.0	0.9	2.4	95.7	0.0	0.5	0.4	90.5	0.0	0.6	1.5
μ	0.0	97.0	1.8	0.7	0.0	92.8	5.2	1.4	0.0	90.1	8.8	0.4
π	0.4	3.8	79.2	10.5	0.4	4.8	60.8	20.2	1.5	6.8	68.2	15.3
ρ	0.1	0.0	7.4	57.5	0.9	0.5	6.3	42.3	1.4	0.7	8.9	37.4
$a_1 \to \pi\ 2\pi^0$	0.0	0.0	0.5	10.3	0.3	0	0.3	11.0	0.3	0.0	1.8	11.3
3 prong	$a_1 \to 3\pi$		$3\pi\pi^0$		$a_1 \to 3\pi$		$3\pi\pi^0$		$a_1 \to 3\pi$		$3\pi\pi^0$	
$a_1 \to 3\pi$	65.1		15.4		69.1		13.3		59.4		10.9	
$3\pi\pi^0$	24.3		48.1		22.5		56.9		27.8		38.6	

Table 1: Efficiencies and misidentification probabilities for various τ decay channels after employing a maximum likelihood selection of exclusive one-prong and three-prong decays.

decay channel $\tau \to \nu_\tau +$	purity (%) barrel	overlap	endcaps
$e\ \bar{\nu}_e$	99.6 ± 0.2	97.9 ± 3.4	95.6 ± 1.7
$\mu\ \bar{\nu}_\mu$	96.9 ± 2.2	96.1 ± 3.5	94.1 ± 5.4
$\pi\ (K)$	78.4 ± 7.1	73.2 ± 8.4	63.4 ± 7.4
$\rho\ (K^*)$	80.3 ± 1.9	67.8 ± 3.8	69.5 ± 3.0
$a_1 \to 3\pi^\pm$	77.5 ± 5.2	73.6 ± 6.9	80.3 ± 5.8

Table 2: Purity of the maximum likelihood selection. The errors include Monte Carlo statistics and systematic uncertainties.

1. the muon-chambers, hadronic calorimeter, presampler, and the $\mathrm{d}E/\mathrm{d}x$ measurement from the jet chamber.

2. the electromagnetic calorimeter only.

Note that these selections have smaller efficiencies and purities than those in which all variables are used. The purities of the test samples can be found in table 3.

type of selection	purity (%) barrel				overlap				endcaps			
(see text)	e	μ	π	ρ	e	μ	π	ρ	e	μ	π	ρ
1.	96.2	95.8	51.2	51.6	93.3	94.3	47.3	50.9	85.5	92.6	39.8	56.7
2.	96.9	87.1	66.3	74.3	86.2	84.6	59.7	67.3	83.3	86.6	49.4	65.3

Table 3: Purities of the test samples of type 1 and 2.

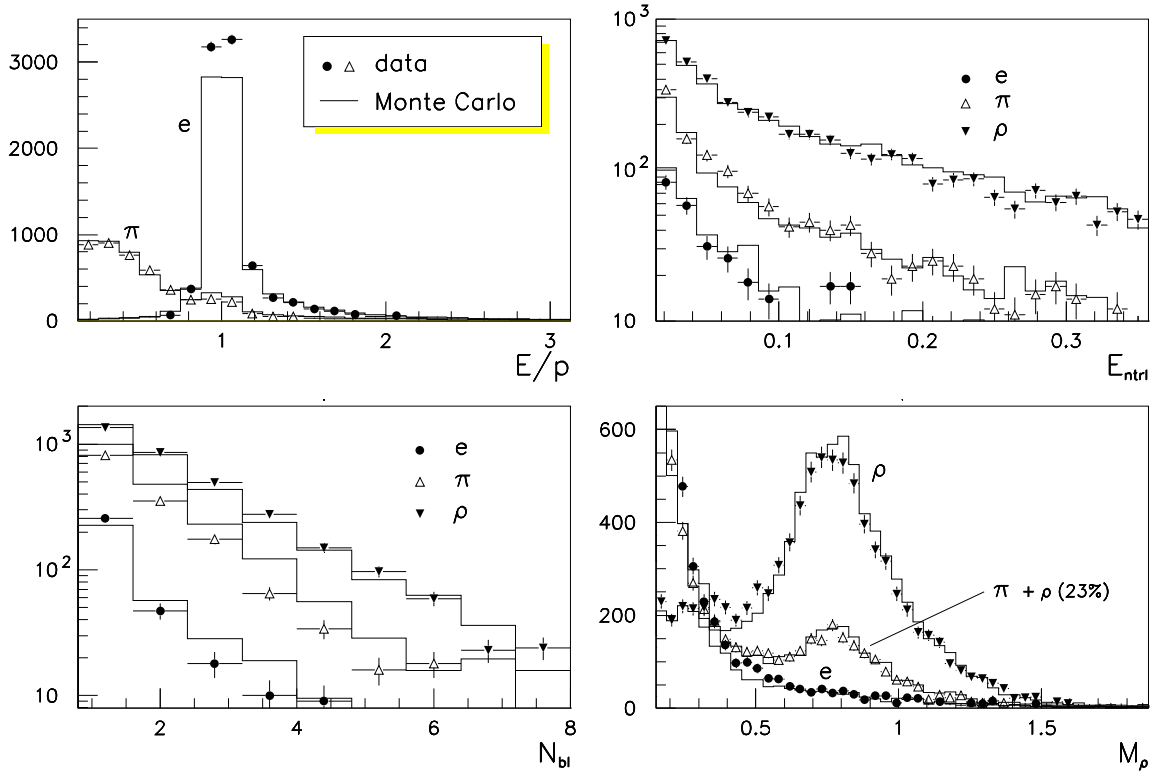

Figure 2: Comparison between data and Monte Carlo simulation using τ decays from the test samples of type 1.

Comparisons between data and Monte Carlo simulation for the most important detector variables are shown in figures 2 and 3. The Monte Carlo distributions compare quite well with the data except for E/p and $N_{\mathrm{hits/layer}}$, where the agreement is only fair. Resulting systematic effects have been estimated by reweighting the Monte Carlo events forcing agreement with the data. The full shift has been assigned as a systematic error (table 2). Generally, the systematic uncertainties were estimated very conservatively because the final measurement of d_τ^w is statistics dominated.

In total, 27 490 events have been selected for the measurement of $\mathrm{Re}(d_\tau^w)$ and 12 834 for $\mathrm{Im}(d_\tau^w)$. Fewer events are used for the measurement of $\mathrm{Im}(d_\tau^w)$ because fewer τ decay modes are used. (See table 4.)

6 The Sensitivities

The sensitivities c_{AB} and f_{AB} in equation (3) are the proportionality constants between the expectation values of the $\mathcal{CP}$-odd observables and the weak dipole moment. Table 4 shows that the hadronic decay channels, which are the most powerful spin analysers in the measurement of the τ-polarization, also have the highest sensitivities.

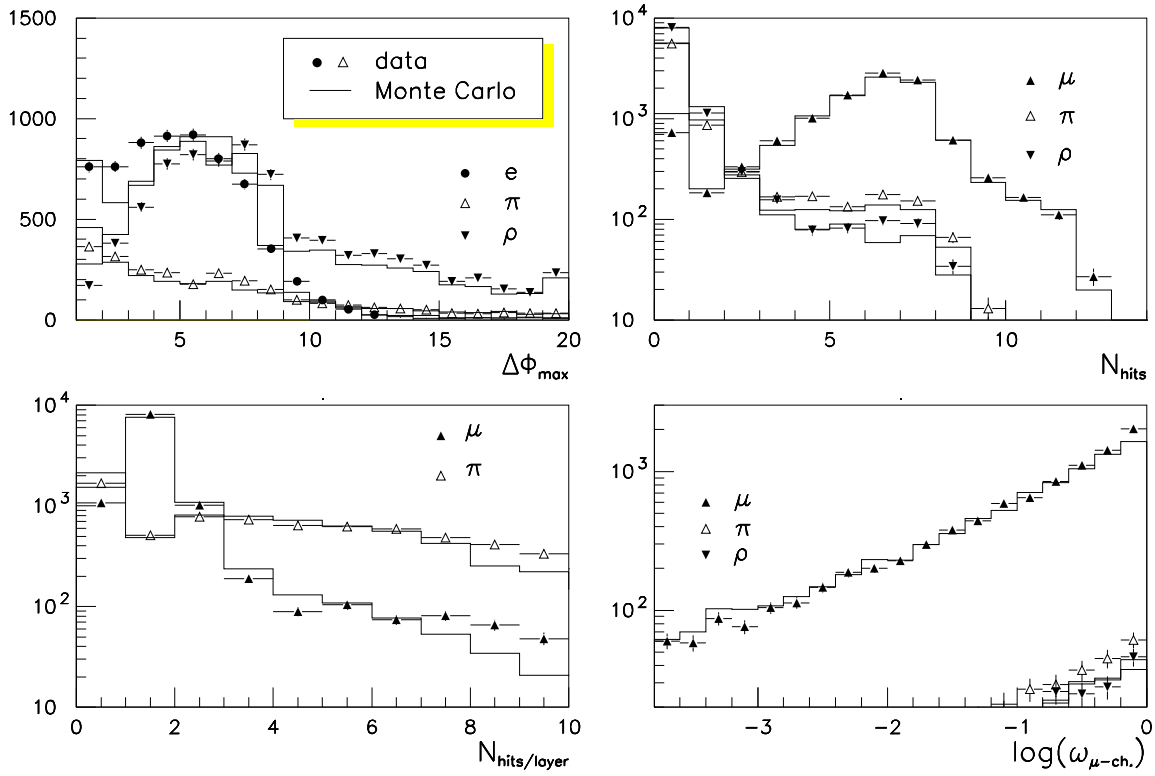

Figure 3: Comparison between data and Monte Carlo simulation using τ decays from the test samples of type 2.

observable	decay channel $\tau^+\tau^- \to$	c_{AB}	f_{AB}
$\mathcal{O}_{\ell\ell}$	$\ell\ell\,\nu_\tau\bar{\nu}_\tau\nu_\ell\bar{\nu}_\ell$	-0.056 ± 0.002	-0.0046 $\pm$ 0.0006
$\mathcal{O}_{\ell\pi}$	$\ell\bar{\pi}\,\nu_\tau\bar{\nu}_\tau\nu_\ell$	0.048 ± 0.002	-
$\mathcal{O}_{\ell\rho}$	$\ell\bar{\rho}\,\nu_\tau\bar{\nu}_\tau\nu_\ell$	0.044 ± 0.002	-
$\mathcal{O}_{\ell 3\pi}$	$\ell\overline{3\pi}\,\nu_\tau\bar{\nu}_\tau\nu_\ell$	0.041 ± 0.004	-
$\mathcal{O}_{\pi\pi}$	$\pi\bar{\pi}\,\nu_\tau\bar{\nu}_\tau$	0.201 ± 0.003	-0.0450 $\pm$ 0.0050
$\mathcal{O}_{\pi\rho}$	$\pi\bar{\rho}\,\nu_\tau\bar{\nu}_\tau$	0.204 ± 0.004	-0.0265 $\pm$ 0.0050
$\mathcal{O}_{\pi 3\pi}$	$\pi\overline{3\pi}\,\nu_\tau\bar{\nu}_\tau$	0.188 ± 0.008	-
$\mathcal{O}_{\rho\rho}$	$\rho\bar{\rho}\,\nu_\tau\bar{\nu}_\tau$	0.211 ± 0.005	-0.0490 $\pm$ 0.0050
$\mathcal{O}_{\rho 3\pi}$	$\rho\overline{3\pi}\,\nu_\tau\bar{\nu}_\tau$	0.195 ± 0.008	-

Table 4: Sensitivities of various τ decay channels for the real part (c_{AB}) and the imaginary part (f_{AB}, some decays only) of the weak dipole moment, before detector cuts. (Errors are from Monte Carlo statistics only.) The $\mathcal{O}_{AB}$ are the optimal observables (9) computed for the respective $\tau^+\tau^- \to A\,\bar{B}\,\nu\bar{\nu}$ decay mode.

The sensitivities can be computed as weighted averages of the $\mathcal{CP}$ observables $\mathcal{O}$ for each decay channel over the appropriate phase space with the differential cross section as a weighting factor. In this phase space integration, the particle momenta are restricted by the

geometrical acceptance of the OPAL detector and the minimal energies are set to the energy cuts used in the data analysis. The sensitivities are functions of $\cos\theta$. Generally they have a maximum absolute value in the overlap region and are lower in the endcaps. The sensitivities of table 4 do not include the influence of detector resolution, background effects or radiative corrections.

Systematic errors of and corrections to the sensitivities of the various τ decay channels arise from other τ decays as well as from non-τ background and from the experimental resolutions of the detector. The influence of radiative corrections, in particular initial state radiation, on the sensitivities is within the bounds of the numerical errors on the sensitivities (about 5%). In order to quantify the effects of the finite energy and momentum resolution on the sensitivities, we compare the $\mathcal{CP}$ observables obtained from generated and reconstructed momenta (see figure 4), the latter taken from the detector simulation. $\mathcal{CP}$-violation was introduced into the standard Monte Carlo [13, 14, 15, 16] by weighting the events according to distributions obtained from a Monte Carlo generator which does include $\mathcal{CP}$-violation (TAUMC [17]) but no detector simulation. The largest reduction (up to 15%) is observed for the sensitivities of decay channels including π^0s in the final state, e.g. $\tau \to \rho\nu \to \pi\pi^0\nu$. The τ decay modes without neutral hadrons are reduced by less than 5%.

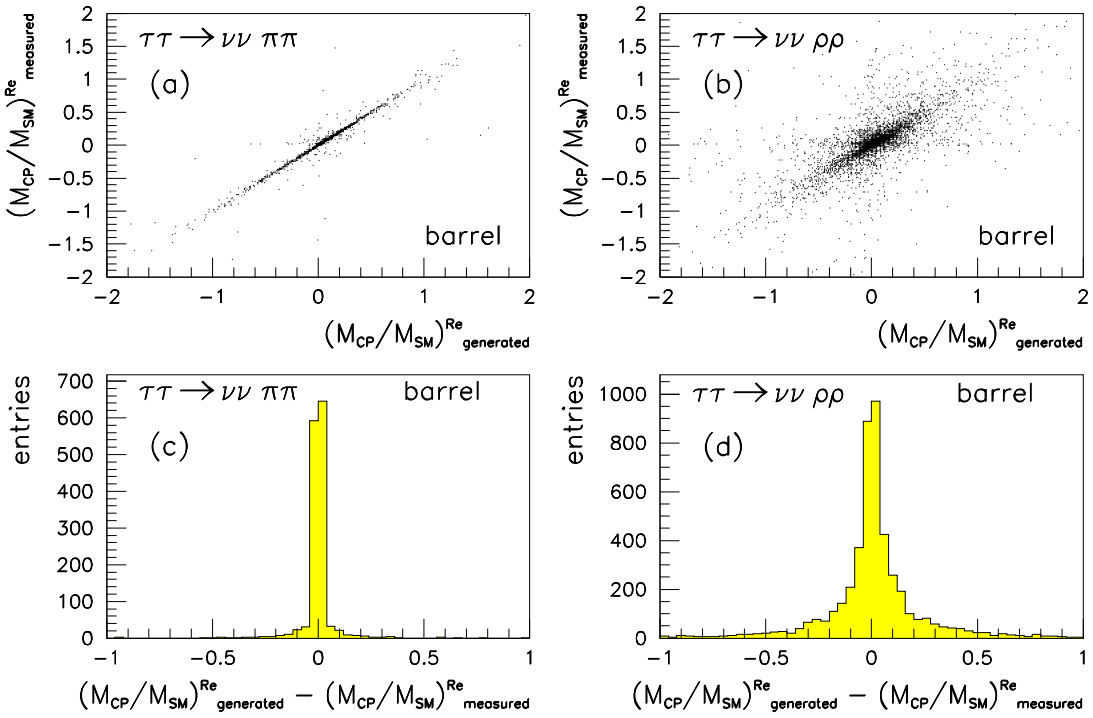

Figure 4: Correlations between generated and measured observables for $\tau^+\tau^- \to \pi^+\pi^-\,\nu\bar{\nu}$ and $\tau^+\tau^- \to \rho^+\rho^-\,\nu\bar{\nu}$ decays (a), (b). The mean values of the difference distributions (c), (d) determine the loss of sensitivity caused by the energy and momentum resolution of the detector.

The non-τ background is assumed to be insensitive to $\mathcal{CP}$-violation effects at the level of the uncertainty discussed here. For the τ-background, however, the influence on the sensitivities is taken into account for each individual channel. Since the $\mathcal{CP}$-odd observables are not optimized for the background decay modes the sensitivities of the τ decay channels are

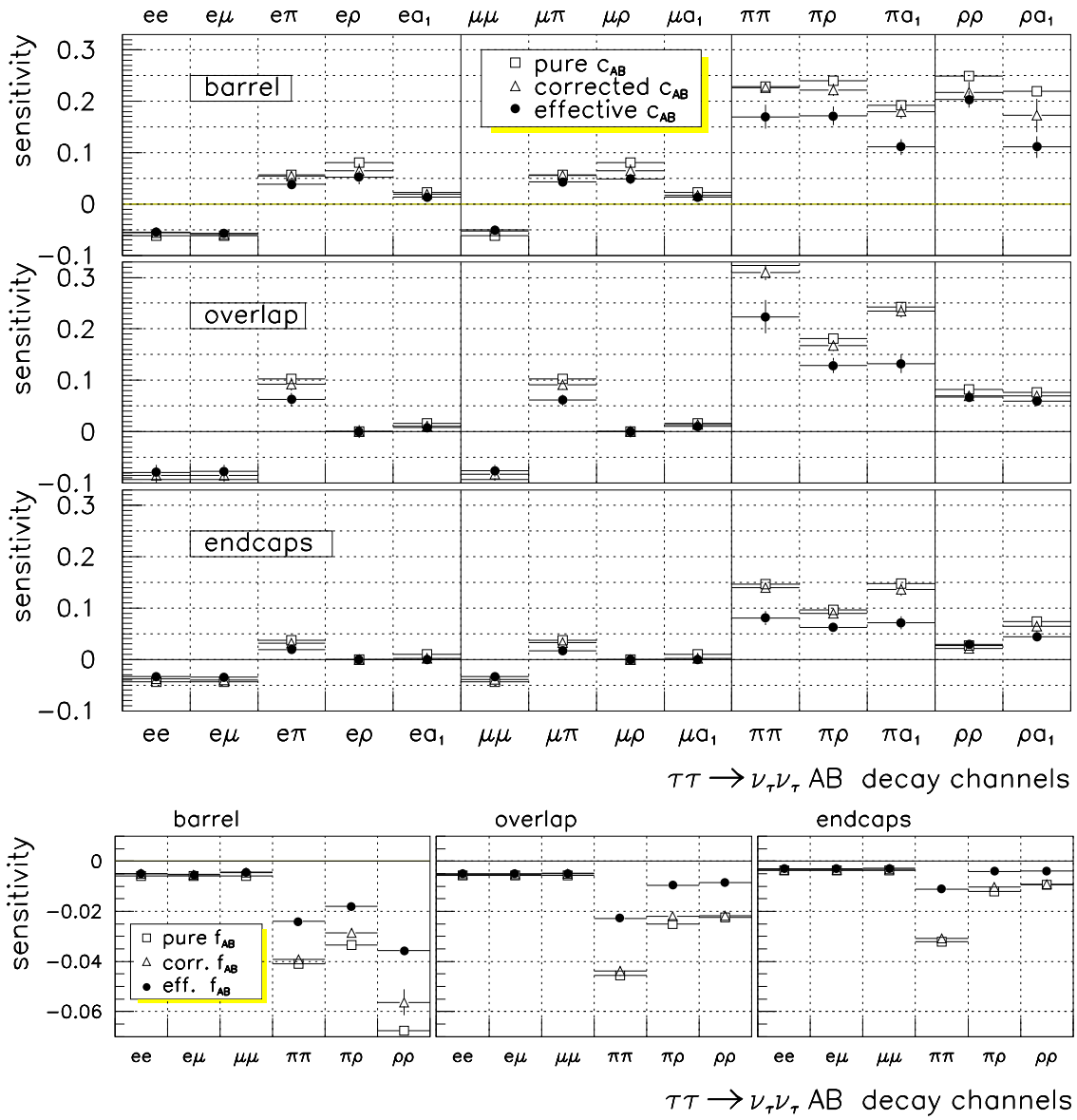

Figure 5: Sensitivities c_{AB} (top) and f_{AB} (bottom) of the $\tau^+\tau^-$ decay modes with respect to the three geometrical regions.

reduced in proportion to their contamination by background sources. This is most evident for the $\tau^+\tau^- \to \pi^+\pi^-\nu\bar{\nu}$ events in the overlap region, where the degradation is about 30% due to the low purity. As mentioned in the previous section, the uncertainties in the quantitative determination of the background sources in the Monte Carlo simulation give rise to systematic errors on the sensitivities. The resulting systematic errors on the sensitivities are below 15%. Figure 5 shows the shifts of the sensitivities, with respect to the estimates of table 4, due to the systematic effects mentioned. The 'pure' c_{AB} and f_{AB} are the original sensitivities calculated by numerical integration. The 'corrected' sensitivities take into account the influence of the energy and momentum resolution of the detector. The 'effective' sensitivities include background effects as well.

7 $\mathcal{CP}$-Symmetry of the Detector

In order to test the validity of our measurements we have investigated the possibility that detector effects could fake CP-violation and hence the existence of a weak dipole moment of the τ. In polar coordinates, leading terms of $M_{\mathcal{CP}}^{\mathrm{Re}}$ are proportional to $\sin(\phi^+ - \phi^-)$ where ϕ is the azimuthal angle of a track in the $x-y$ plane. $M_{\mathcal{CP}}^{\mathrm{Im}}$ shows an approximate proportionality to the difference of the tracks' polar angles, $\cos(\theta^+ - \theta^-)$. These relations indicate how $\mathcal{CP}$-violation could be faked. If a systematic rotation of one side of the detector with respect to the opposite side exists, for example a systematic rotation of the two drift chamber end cones or the endcaps of the electromagnetic calorimeter with respect to each other, the distorted azimuth could lead to a non-zero mean value $\langle \sin(\phi^+ - \phi^-) \rangle$. Similarly, a systematic mismeasurement of one or both polar angles could give rise to a non-zero $\langle \cos(\theta^+ - \theta^-) \rangle$ and hence to a non-zero imaginary part of the dipole moment. In order to study this possibility we calculated the $\mathcal{CP}$-odd observables using events for which $\mathcal{CP}$-violation originating from the reaction itself can be excluded. The $\mathcal{CP}$-symmetry of the tracking chambers can be studied using $e^+e^- \to \mu^+\mu^-$ events. Using about 38 700 of these events we find no deviation from zero within the statistical errors, for all observables considered and in the three geometrical regions of the detector. The precisions with which zero mean values could be reproduced were taken as the systematic errors of the observables and are given in table 5 and 6 ($\Delta^{\mathrm{sys}}\langle \mathcal{O}^{\mathcal{T}^\pm} \rangle$). $\mathcal{CP}$-violation arising from instrumental effects of the electromagnetic calorimeter or its alignment with the tracking chamber has also been studied; in the reconstruction of the ρ channel the electromagnetic calorimeter is used to measure the π^0. Artificially constructed $\tau^+\tau^- \to (\pi^+\pi^0)\,(\pi^-\pi^0)\,\nu_\tau\bar{\nu}_\tau$ events, formed by combining a $\tau^+ \to \pi^+\pi^0\nu$ decay from one event with a $\tau^- \to \pi^-\pi^0\nu$ decay from another event are used. These events are uncorrelated and can therefore not give rise to any $\mathcal{CP}$-violation by a physical interaction. The $\mathcal{CP}$ measurement applied to these mixed events shows no deviation from zero. (See table 5,6)

In summary, using intrinsically $\mathcal{CP}$-symmetric events the expectation values of all observables are consistent with zero. The errors on the mean values were always much smaller than the ones obtained for the $\tau^+\tau^-$ events. We therefore conclude that the detector is CP-symmetric to a level of $\mathrm{Re}(d_\tau^{\mathrm{detector}}) < 4 \times 10^{-19}$ e·cm and $\mathrm{Im}(d_\tau^{\mathrm{detector}}) < 3 \times 10^{-18}$ e·cm, respectively, i.e. 19 and 14 times better than the limits reported here.

8 Results

The distributions of the $\mathcal{CP}$-odd observables derived from the selected events are shown in figures 6 and 8. Using equation (3) the real and imaginary parts of the weak dipole moment of the τ can be determined by measuring the mean values of the CP-observables. Table 5 shows the effective sensitivities for the real part of the weak dipole moment obtained for the τ decay channels considered and table 6 for the imaginary part. The final values are obtained by calculating the weighted mean of the real and the imaginary parts of the weak dipole moment using Gaussian error propagation for the statistical and the non-correlated part of the systematic errors. The systematic errors of the sensitivities arising from detector resolution effects and $\Delta^{\mathrm{sys}}\langle \mathcal{O}^{\mathcal{T}^\pm} \rangle$ are treated as correlated errors. The resulting errors are finally summed up quadratically with the non-correlated errors. The measured dipole moments are plotted in figures 7 and figures 9.

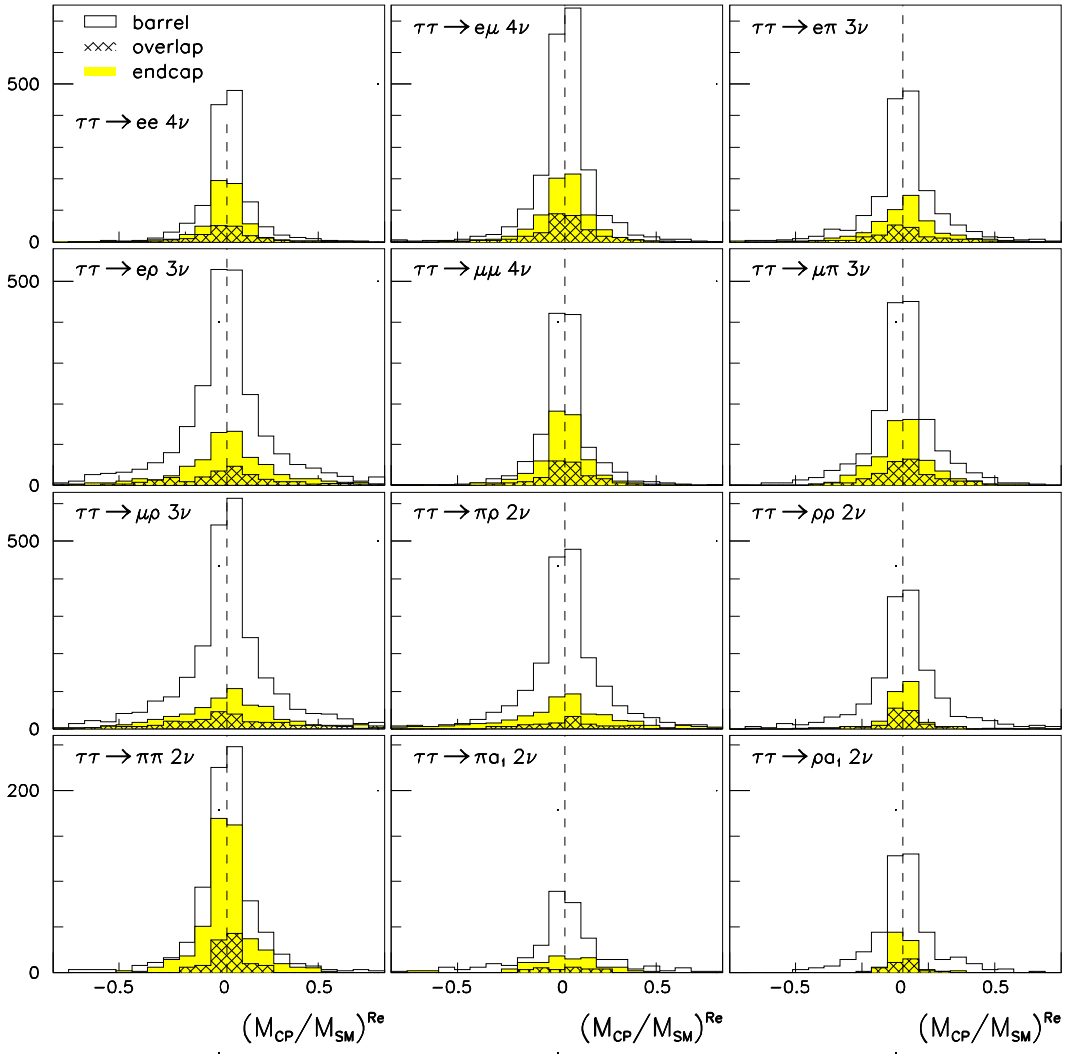

Figure 6: The measured $\mathcal{CP}$-odd, $\mathcal{T}$-odd observables from $Z^0 \to \tau^+\tau^-$ events of the 1991, 1992 and 1993 data.

In total, we obtain for the real part of the weak dipole moment

$$\mathrm{Re}(d_\tau^w) \;=\; (\; -0.2 \;\pm\; 3.6 \;\pm\; 1.4\;) \times 10^{-18}\; e\cdot\mathrm{cm}\;, \tag{12}$$

where the errors are due to statistical fluctuations (first number) and systematic uncertainties (second number). The value is consistent with zero, resulting in an upper limit of

$$|\mathrm{Re}(d_\tau^w)| \;<\; 7.8 \times 10^{-18}\; e\cdot\mathrm{cm} \tag{13}$$

at the 95% confidence level.

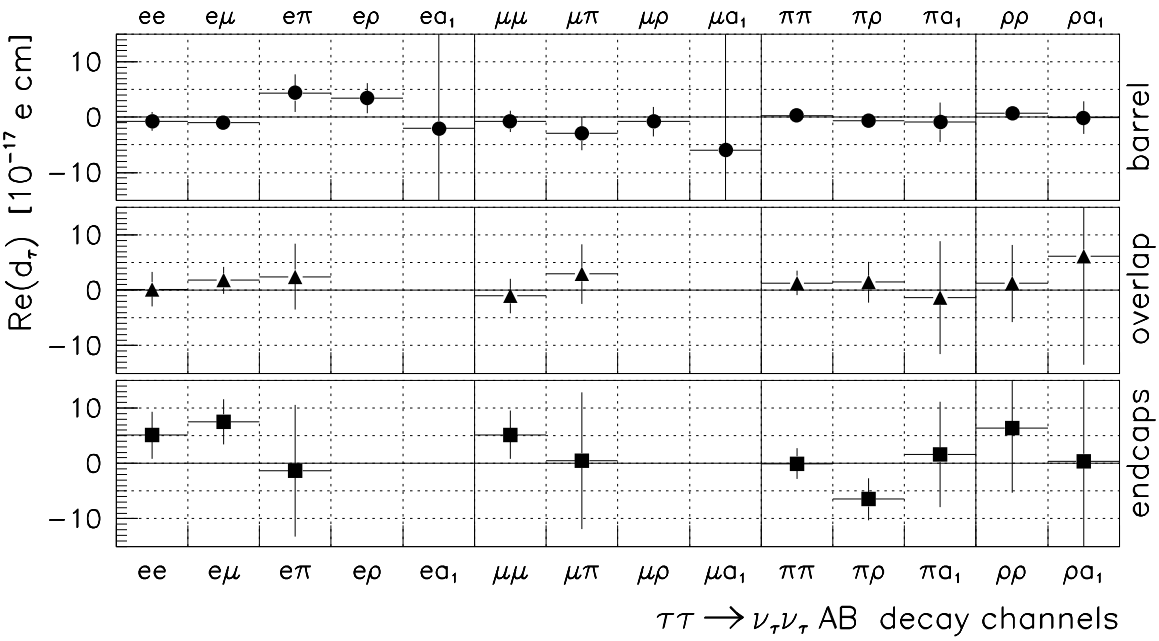

Figure 7: The real part of the weak dipole moment in the considered $\tau^+\tau^-$ decay channels with respect to the three geometrical regions.

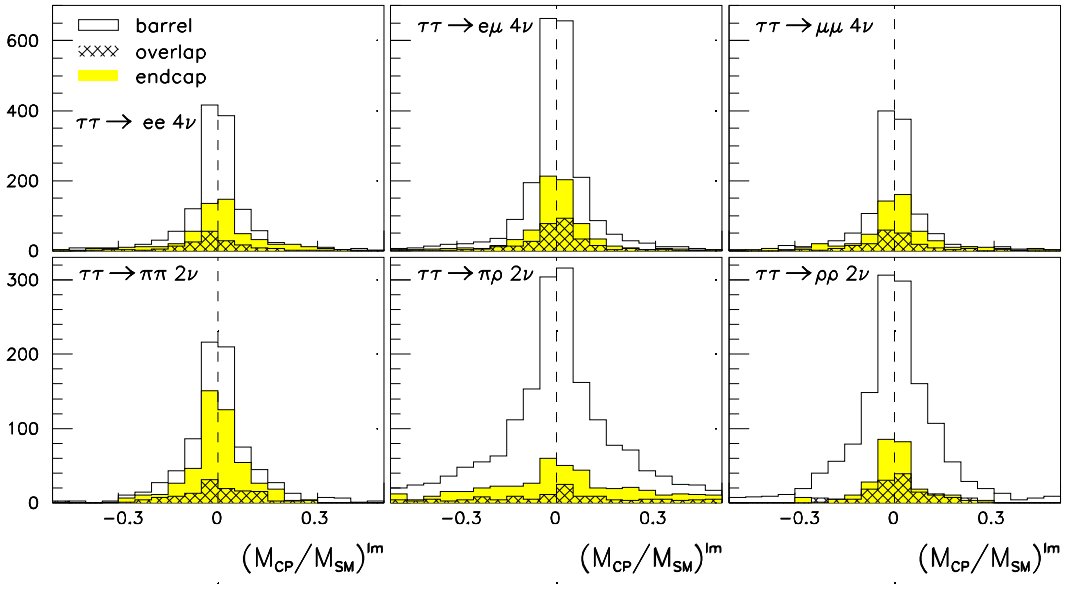

Figure 8: The measured $\mathcal{CP}$-odd, $\mathcal{T}$-even observables from $Z^0 \to \tau^+\tau^-$ events of the 1991, 1992 and 1993 data.

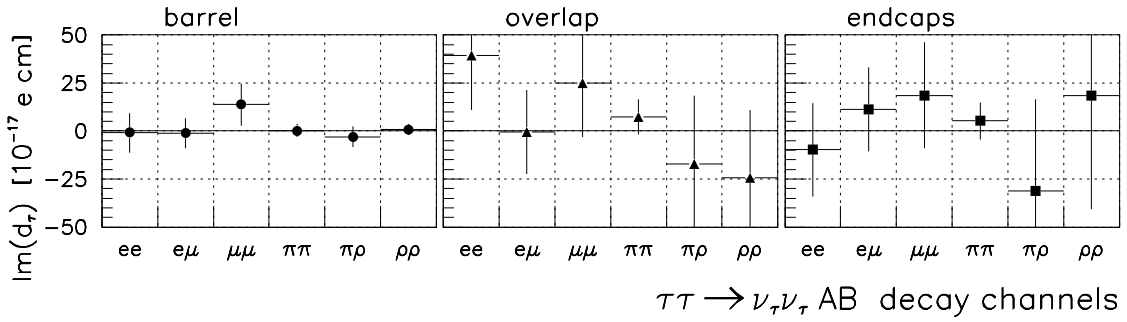

Figure 9: The imaginary part of the weak dipole moment in the considered $\tau^+\tau^-$ decay channels with respect to the three geometrical regions.

For the imaginary part of the weak dipole moment we obtain

$$\mathrm{Im}(d_\tau^w) \;=\; (\;0.95 \;\pm\; 1.55 \;\pm\; 0.91\;) \times 10^{-17}\; e \cdot \mathrm{cm}\;, \tag{14}$$

again consistent with zero, resulting in an upper limit of

$$|\mathrm{Im}(d_\tau^w)| \;<\; 4.5 \times 10^{-17}\; e \cdot \mathrm{cm} \tag{15}$$

with 95% confidence. Since the sensitivities f_{AB} have not been calculated for all selected $\tau^+\tau^-$ decay modes (see table 4) a factor of about 2.1 higher statistics was used in the determination of $\mathrm{Re}(d_\tau^w)$ compared to $\mathrm{Im}(d_\tau^w)$. Generally, the signal-to-noise ratio of the $\mathcal{CP}$-odd and $\mathcal{T}$-even observables is about 1.4 times lower than the $\mathcal{CP}$-odd and $\mathcal{T}$-odd observables. Therefore one expects a larger statistical error in the measurement of the imaginary part of the weak dipole moment. In both cases $\Delta_{\mathrm{sys}}/\Delta_{\mathrm{stat}}$ is below 60%.

This analysis sets a new upper limit on the real part of the $\mathcal{CP}$-violating weak dipole moment and, for the first time, on the imaginary part of the weak dipole moment. The introduction of new, more sensitive $\mathcal{CP}$-odd observables resulted in a reduction of the statistical errors by up to a factor 2.2 compared to observables used in former analyses [5, 6].

decay channel	θ	$c^{\rm eff} \pm \Delta c^{\rm eff}$	$\langle \mathcal{O}^{\mathcal{T}^-} \rangle \pm \Delta^{\rm stat}\langle \mathcal{O}^{\mathcal{T}^-} \rangle \pm \Delta^{\rm sys}\langle \mathcal{O}^{\mathcal{T}^-} \rangle$	$\mathrm{Re}(d_\tau^w) \pm \Delta\mathrm{Re}(d_\tau^w)$	$\Delta^{\rm stat} d_\tau^w$	$\Delta^{\rm sys} d_\tau^w$
$e-e$	B	-0.0550 ± 0.0067	0.0018 ± 0.0043 ± 0.0002	-0.71 ± 1.70	1.69	0.12
	O	-0.0794 ± 0.0148	-0.0007 ± 0.0113 ± 0.0004	0.19 ± 3.09	3.09	0.11
	E	-0.0330 ± 0.0039	-0.0078 ± 0.0064 ± 0.0004	5.12 ± 4.26	4.20	0.66
$e-\mu$	B	-0.0572 ± 0.0056	0.0027 ± 0.0033 ± 0.0002	-1.02 ± 1.25	1.24	0.13
	O	-0.0774 ± 0.0125	-0.0064 ± 0.0088 ± 0.0004	1.79 ± 2.48	2.46	0.31
	E	-0.0340 ± 0.0070	-0.0118 ± 0.0059 ± 0.0004	7.53 ± 4.08	3.76	1.57
$e-\pi$	B	0.0387 ± 0.0047	0.0077 ± 0.0060 ± 0.0002	4.31 ± 3.41	3.36	0.53
	O	0.0626 ± 0.0132	0.0071 ± 0.0171 ± 0.0005	2.46 ± 5.95	5.92	0.54
	E	0.0194 ± 0.0036	-0.0012 ± 0.0106 ± 0.0003	-1.34 ± 11.86	11.84	0.42
$e-\rho$	B	0.0518 ± 0.0127	-0.0082 ± 0.0061 ± 0.0003	-3.43 ± 2.69	2.55	0.85
	O	-	-0.0039 ± 0.0181 ± 0.0005	-	-	-
	E	-	0.0091 ± 0.0115 ± 0.0004	-	-	-
$e-a_1$	B	0.0139 ± 0.0054	-0.0013 ± 0.0143 ± 0.0002	-2.02 ± 22.34	24.96	0.85
	O	0.0079 ± 0.0061	0.0176 ± 0.0384 ± 0.0005	48.34 ± 111.89	105.49	37.32
	E	-	-0.0082 ± 0.0194 ± 0.0003	-	-	-
$\mu-\mu$	B	-0.0499 ± 0.0054	0.0018 ± 0.0044 ± 0.0002	-0.78 ± 1.91	1.91	0.12
	O	-0.0756 ± 0.0115	0.0036 ± 0.0108 ± 0.0004	-1.03 ± 3.10	3.09	0.19
	E	-0.0329 ± 0.0050	-0.0078 ± 0.0065 ± 0.0004	5.14 ± 4.37	4.29	0.83
$\mu-\pi$	B	0.0435 ± 0.0049	-0.0059 ± 0.0060 ± 0.0002	-2.94 ± 3.01	2.99	0.34
	O	0.0616 ± 0.0107	0.0084 ± 0.0152 ± 0.0005	2.95 ± 5.38	5.45	0.54
	E	0.0172 ± 0.0034	0.0004 ± 0.0098 ± 0.0003	0.50 ± 12.37	12.33	0.39
$\mu-\rho$	B	0.0486 ± 0.0103	-0.0018 ± 0.0060 ± 0.0003	-0.80 ± 2.68	2.67	0.22
	O	-	0.0166 ± 0.0168 ± 0.0005	-	-	-
	E	-	0.0060 ± 0.0117 ± 0.0004	-	-	-
$\mu-a_1$	B	0.0138 ± 0.0054	-0.0038 ± 0.0153 ± 0.0002	-5.97 ± 24.17	18.64	2.35
	O	0.0104 ± 0.0064	-0.0148 ± 0.0263 ± 0.0005	-30.88 ± 58.08	54.87	19.03
	E	-	-0.0226 ± 0.0264 ± 0.0003	-	-	-
$\pi-\pi$	B	0.1699 ± 0.0231	0.0023 ± 0.0082 ± 0.0002	0.29 ± 1.04	0.92	0.47
	O	0.2238 ± 0.0327	0.0137 ± 0.0223 ± 0.0007	1.32 ± 2.17	2.16	0.20
	E	0.0801 ± 0.0136	-0.0001 ± 0.0104 ± 0.0002	-0.03 ± 2.81	2.81	0.05
$\pi-\rho$	B	0.1713 ± 0.0181	-0.0052 ± 0.0056 ± 0.0003	-0.66 ± 0.71	0.70	0.08
	O	0.1288 ± 0.0153	0.0086 ± 0.0222 ± 0.0008	1.45 ± 3.74	3.73	0.22
	E	0.0621 ± 0.0078	-0.0186 ± 0.0106 ± 0.0003	-6.49 ± 3.79	3.70	0.82
$\pi-a_1$	B	0.1110 ± 0.0155	-0.0047 ± 0.0169 ± 0.0002	-0.92 ± 3.53	3.53	0.14
	O	0.1321 ± 0.0185	-0.0084 ± 0.0620 ± 0.0007	-1.37 ± 10.19	10.19	0.22
	E	0.0714 ± 0.0121	0.0052 ± 0.0313 ± 0.0002	1.58 ± 9.51	9.51	0.27
$\rho-\rho$	B	0.2036 ± 0.0162	0.0065 ± 0.0074 ± 0.0004	0.69 ± 0.79	0.78	0.07
	O	0.0673 ± 0.0056	0.0039 ± 0.0216 ± 0.0009	1.25 ± 6.97	6.96	0.31
	E	0.0289 ± 0.0027	0.0085 ± 0.0155 ± 0.0004	6.38 ± 11.65	11.63	0.67
$\rho-a_1$	B	0.1110 ± 0.0211	-0.0003 ± 0.0151 ± 0.0003	-0.06 ± 2.95	2.95	0.06
	O	0.0591 ± 0.0065	0.0168 ± 0.0533 ± 0.0008	6.16 ± 19.58	19.57	0.74
	E	0.0438 ± 0.0062	0.0008 ± 0.0335 ± 0.0003	0.39 ± 16.59	16.58	0.16

Table 5: Measurements of the real part of the weak dipole moment for the respective τ decay channels in the three geometrical regions of the OPAL detector. In addition, the effective sensitivities are given, including detector and background corrections. $\Delta^{\rm sys}\langle \mathcal{O}^{\mathcal{T}^\pm} \rangle$ are the systematic errors arising from limits on $\mathcal{CP}$-violation effects in the detector.

decay channel	θ	$f^{\rm eff} \pm \Delta f^{\rm eff}$	$\langle \mathcal{O}^{T^+} \rangle \pm \Delta^{\rm stat}\langle \mathcal{O}^{T^+} \rangle \pm \Delta^{\rm sys}\langle \mathcal{O}^{T^+} \rangle$	$\mathrm{Im}(d_\tau^w) \pm \Delta\mathrm{Im}(d_\tau^w)$	$\Delta^{\rm stat} d_\tau^w$	$\Delta^{\rm sys} d_\tau^w$
$e-e$	B	-0.0051 ± 0.0006	0.0002 ± 0.0022 ± 0 .0010	-0.85 ± 10.28	9.36	4.25
	O	-0.0049 ± 0.0006	-0.0089 ± 0.0059 ± 0 .0023	39.41 ± 28.45	26.12	11.27
	E	-0.0031 ± 0.0004	0.0014 ± 0.0033 ± 0 .0011	-9.80 ± 24.38	23.09	7.80
$e-\mu$	B	-0.0052 ± 0.0006	0.0003 ± 0.0016 ± 0 .0010	-1.25 ± 7.87	6.67	4.18
	O	-0.0050 ± 0.0008	0.0001 ± 0.0045 ± 0 .0023	-0.43 ± 21.93	19.53	9.98
	E	-0.0031 ± 0.0006	-0.0016 ± 0.0029 ± 0 .0011	11.2 ± 21.81	20.29	8.00
$\mu-\mu$	B	-0.0044 ± 0.0009	-0.0028 ± 0.0023 ± 0 .0010	13.81 ± 10.91	9.32	5.68
	O	-0.0048 ± 0.0010	-0.0055 ± 0.0056 ± 0 .0023	24.86 ± 27.85	32.31	11.61
	E	-0.0028 ± 0.0008	-0.0024 ± 0.0033 ± 0 .0011	18.6 ± 27.48	25.57	10.05
$\pi-\pi$	B	-0.0239 ± 0.0035	-0.0003 ± 0.0037 ± 0 .0002	0.27 ± 3.36	3.36	0.19
	O	-0.0228 ± 0.0045	-0.0076 ± 0.0095 ± 0 .0004	7.23 ± 9.16	9.04	1.48
	E	-0.0112 ± 0.0027	-0.0027 ± 0.0049 ± 0 .0002	5.23 ± 9.58	9.49	1.32
$\pi-\rho$	B	-0.0180 ± 0.0019	0.0025 ± 0.0044 ± 0 .0003	-3.01 ± 5.31	5.30	0.38
	O	-0.0097 ± 0.0013	0.0077 ± 0.0159 ± 0 .0005	-17.23 ± 35.66	35.57	2.56
	E	-0.0041 ± 0.0005	0.0059 ± 0.0090 ± 0 .0003	-31.22 ± 47.81	40.62	4.13
$\rho-\rho$	B	-0.0356 ± 0.0033	-0.0015 ± 0.0043 ± 0 .0004	0.91 ± 2.63	2.62	0.26
	O	-0.0085 ± 0.0005	0.0095 ± 0.0137 ± 0 .0006	-24.25 ± 35.04	34.97	2.09
	E	-0.0040 ± 0.0004	-0.0034 ± 0.0109 ± 0 .0004	18.44 ± 59.20	59.13	2.84

Table 6: Same as table 5 for the imaginary part of the weak dipole moment.

Acknowledgements

We gratefully acknowledge numerous helpful discussions with P. Overmann, W. Bernreuther and O. Nachtmann.

It is a pleasure to thank the SL Division for the efficient operation of the LEP accelerator, the precise information on the absolute energy, and their continuing close cooperation with our experimental group. In addition to the support staff at our own institutions we are pleased to acknowledge the
Department of Energy, USA,
National Science Foundation, USA,
Particle Physics and Astronomy Research Council, UK,
Natural Sciences and Engineering Research Council, Canada,
Fussefeld Foundation,
Israel Ministry of Science,
Israel Science Foundation, administered by the Israel Academy of Science and Humanities,
Minerva Gesellschaft,
Japanese Ministry of Education, Science and Culture (the Monbusho) and a grant under the Monbusho International Science Research Program,
German Israeli Bi-national Science Foundation (GIF),
Direction des Sciences de la Matière du Commissariat à l'Energie Atomique, France,
Bundesministerium für Forschung und Technologie, Germany,
National Research Council of Canada,
A.P. Sloan Foundation and Junta Nacional de Investigação Científica e Tecnológica, Portugal.

Appendix: Tau Spin and Flight Direction

Neither the τ spin nor the τ flight direction can be measured directly. However, in the reaction $e^+e^- \longrightarrow \tau^+(k^+)\,\tau^-(k^-) \longrightarrow A^+(p_A)\,B^-(p_B)\,\nu_\tau\bar{\nu}_\tau$ the τ momentum $\hat{\mathbf{k}}$ can be reconstructed up to a twofold ambiguity assuming two-body kinematics and assuming that the Z^0 rest frame corresponds to the laboratory frame which means that initial state radiation is neglected. The ambiguity can be resolved in principle by means of the information obtained from a precise vertex detector measuring the track positions close to the interaction point in three dimensions as proposed in [18]. This would increase our sensitivity to $\mathcal{CP}$-violation by approximately 10%. We currently reconstruct only the component of the τ^+ momentum in the decay plane of the final state particles. Considering the decay $\tau^+\tau^- \to A\,B\,\nu_\tau\bar{\nu}_\tau$ it is given by

$$\mathbf{k} \;=\; u\hat{\mathbf{p}}_A \;+\; v\hat{\mathbf{p}}_B \tag{16}$$

$$u \;=\; \frac{\alpha_A \;+\; \hat{\mathbf{p}}_A{\cdot}\hat{\mathbf{p}}_B\alpha_B}{1 \;-\; (\hat{\mathbf{p}}_A{\cdot}\hat{\mathbf{p}}_B)^2} \quad , \qquad v \;=\; -\frac{\alpha_B \;+\; \hat{\mathbf{p}}_A{\cdot}\hat{\mathbf{p}}_B\alpha_A}{1 \;-\; (\hat{\mathbf{p}}_A{\cdot}\hat{\mathbf{p}}_B)^2} \quad , \tag{17}$$

where hats denote unit momenta in the laboratory frame, and

$$\alpha_i \;=\; \frac{\sqrt{s} \;-\; m_\tau^2 \;-\; m_i^2}{2|\mathbf{p}_i|} \qquad (i \;=\; A,\; B)\;, \tag{18}$$

where $\sqrt{s}$ is the c.m. energy and m_τ ($m_{A/B}$) is the mass of the τ-lepton (invariant mass of the final state particles A and B, respectively).

As pointed out in [19, 14], the differential partial width for any decay of a polarized τ is $\mathrm{d}\Gamma = |\bar{M}|^2/2m_\tau \cdot (1 + \mathbf{S}\,\mathbf{h})\,\mathrm{d}PS$, where $|\bar{M}|^2$ is the squared matrix element and $\mathbf{S}$ is the three-dimensional polarization vector in the τ rest frame. If the τ momentum $\mathbf{k}$ is known, the *polarimeter vector* $\mathbf{h}$ can be computed from the momentum of the daughter particles in the laboratory frame [20]. In this analysis the τ decay modes into $e\,\nu\bar{\nu}$, $\mu\,\nu\bar{\nu}$, $\pi\,\nu$, $\pi\pi^0\,\nu$, $3\pi\,\nu$ are selected exclusively. The condition of maximum emission probability means that we use for the spin orientation the direction of the polarimeter vector, which leads us to the expressions [7]:

$$[\mathbf{S}^\pm]_{\tau\to\ell\nu_\ell\nu} \;=\; -m_\tau\frac{\pm\,(2(k^\pm p_\ell^\pm - m_\ell^2)(h^\pm - g^\pm) + \frac{1}{2}g^\pm(f^\pm + m_\tau^2 - m_\ell^2))\cdot\mathbf{k} - f^\pm\mathbf{p}_\ell^\pm}{(k^\pm p_\ell^\pm)\,(3m_\tau^2 + 3m_\ell^2 - 4k^\pm p_\ell^\pm) \;-\; 2m_\tau m_\ell}\;,$$

where

$$f^\pm = m_\tau^2 + 3m_\ell^2 - 4k^\pm p_\ell^\pm \;, \quad g^\pm = \frac{E_\ell^\pm}{m_\tau} - \frac{k^\pm p_\ell^\pm}{m_\tau(k_0 + m_\tau)}$$

$$h^\pm = \frac{E_\ell^\pm}{m_\tau} - 1 - \frac{(k_0)^2 - m_\tau^2}{m_\tau(k_0 + m_\tau)}$$

$p_\ell = (E_\ell,\ \mathbf{p}_\ell)$ is the four – momentum of the outgoing lepton.

$k \;= (k_0,\ \mathbf{k})$ that of the τ

$$[\mathbf{S}^\pm]_{\tau\to\pi\nu} \;=\; \frac{2}{m_\tau^2 \;-\; m_\pi^2}\left(\mp m_\tau\mathbf{p}_{\pi^\pm} \;+\; \frac{m_\tau^2 \;+\; m_\pi^2 \;+\; 2m_\tau E_{\pi^\pm}}{2(k_0 \;+\; m_\tau)}\mathbf{k}\right)$$

$$[\mathbf{S}^\pm]_{\tau\to\rho\nu\to\pi\pi^0\nu} \;=\; \mp\,\frac{\mp H_0^\pm\mathbf{k} \;+\; m_\tau\mathbf{H}^\pm \;+\; \mathbf{k}\cdot(\mathbf{k}{\cdot}\mathbf{H}^\pm)/(k_0 \;+\; m_\tau)}{(k^\pm H^\pm) \;-\; m_\tau^2\cdot(p_{\pi^\pm} \;-\; p_{\pi^0})^2}\;,$$

where

$$(H^{\pm})^{\nu} = \quad 2(p_{\pi^{\pm}} - p_{\pi^0})^{\nu}(p_{\pi^{\pm}} - p_{\pi^0})^{\mu}(k_{\pm})_{\mu} + (p_{\pi^{\pm}} + p_{\pi^0})^{\nu}(p_{\pi^{\pm}} - p_{\pi^0})^2$$

and $p_{\pi^{\pm}}$ and p_{π^0} are the four – momenta of the charged and neutral pions, respectively.

The expression for the 3π decay channel follows the notation

$$\tau^{\pm}(k) \longrightarrow (a_1\nu \to \rho\pi\nu) \longrightarrow \pi^{\mp}(p^{\mp})\,\pi^{\pm}(p_1)\,\pi^{\pm}(p_2)$$

which is equivalent to a decay into a charged and two neutral pions by rotation of isospin assuming isospin invariance[2]. One obtains

$$[\mathbf{S}^{\pm}]_{\tau\to a_1\nu\to\rho\pi\nu\to 3\pi\nu} = \mp m_{\tau}\,(\mathbf{Z}^{\pm}/N^{\pm})\,, \tag{19}$$

where

$$\mathbf{Z}^{\pm} = \Big[\,\Big(|F_{\rho}^1|^2\,(kh_1) + \mathrm{Re}(F_{\rho}^1F_{\rho}^2)\,(kh_2)\Big)\,\boldsymbol{\xi}_1 + \Big(|F_{\rho}^2|^2\,(kh_2) + \mathrm{Re}(F_{\rho}^1F_{\rho}^2)\,(kh_1)\Big)\,\boldsymbol{\xi}_2 - \frac{1}{2}(h_1h_2)\,\mathrm{Re}(F_{\rho}^1 + F_{\rho}^2)^2\,\boldsymbol{\eta} + \mathrm{Im}(F_{\rho}^1F_{\rho}^2)\,\boldsymbol{\zeta}\,\Big]^{\pm}$$

$$N^{\pm} = \Big[\,\mathrm{Re}\Big(F_{\rho}^1(kh_1) + F_{\rho}^2(kh_2)\Big)^2 - \frac{1}{2}\,k(k-Q)\,(h_1h_2)\,\mathrm{Re}(F_{\rho}^1 + F_{\rho}^2)^2 + \mathrm{Im}(F_{\rho}^1F_{\rho}^2)\,(kH)\,\Big]^{\pm}\,.$$

Here, we used the definitions

$$\boldsymbol{\xi}^{\pm}{}_{1/2} = \mathbf{Y}^{\pm}(h_{1/2}^{\pm})\,, \quad \boldsymbol{\eta}^{\pm} = \mathbf{Y}^{\pm}(k^{\pm} - Q^{\pm})\,, \quad \boldsymbol{\zeta}^{\pm} = \mathbf{Y}^{\pm}(H^{\pm})$$

and

$$\mathbf{Y}^{\pm} = \mathbf{Y}^{\pm}(b) = \pm\frac{b^0}{m_{\tau}}\mathbf{k} - \mathbf{b} - \frac{\mathbf{k}\cdot\mathbf{b}}{m_{\tau}(E_{\tau}+m_{\tau})}\mathbf{k}\,, \qquad b = b\,(b^0,\mathbf{b})\,.$$

The four-vector $H^{\pm}$ arises from permutation terms in the $\tau \to 3\pi$ decay matrix and is given by

$$H^{\pm} = \begin{pmatrix} (k-Q)_2\lambda_{13} + (k-Q)_1\lambda_{32} + (k-Q)_3\lambda_{21} \\ (k-Q)_3\lambda_{02} + (k-Q)_0\lambda_{23} + (k-Q)_2\lambda_{30} \\ (k-Q)_0\lambda_{31} + (k-Q)_3\lambda_{10} + (k-Q)_1\lambda_{03} \\ (k-Q)_1\lambda_{20} + (k-Q)_2\lambda_{01} + (k-Q)_0\lambda_{12} \end{pmatrix}^{\pm}$$

where

$$\lambda_{\mu\nu}^{\pm} = (h_{\mu}^1h_{\nu}^2 - h_{\nu}^1h_{\mu}^2)^{\pm}$$

[2]In this case the notation follows $\tau^{\pm}(k) \to \pi^{\pm}(p^{\pm})\ \pi^0(p_1)\ \pi^0(p_2)$.

and

$$h^{\pm}_{1/2} \;=\; \left[\, p - p_{1/2} - Q\frac{Q(p-p_{1/2})}{(Q)^2} \,\right]^{\pm} , \qquad Q^{\pm} \;=\; p^{\pm} + p_1 + p_2 \;.$$

$F^{1/2}_{\rho^{\pm}} \;=\; F_\rho\left((p^{\pm} + p_{1/2})^2\right)$ is the Breit-Wigner propagator describing the ρ resonance

$$F_\rho(u) \;=\; \frac{m^2_\rho}{m^2_\rho - u - i\sqrt{u}\Gamma(u)}$$

which contains the momentum dependent, p-wave corrected width

$$\Gamma(u) \;=\; \Gamma_\rho \,\frac{m^2_\rho}{(m^2_\rho - 4m^2_\pi)^{3/2}}\,\frac{(u-4m^2_\pi)^{3/2}}{u} \;.$$

In these expressions the vector $\mathbf{k}$ describes the real τ flight direction, but in the following measurement it is replaced by the approximation given in equation (16).

References

[1] M. Kobayashi and T. Maskawa, *Prog. Theor. Phys.* **49** (1973) 652.

[2] W. Bernreuther, U. Löw, J. P. Ma, O. Nachtmann, *Z. Phys.* **C 43** (1989) 117.

[3] W. Bernreuther, O. Nachtmann, *Phys. Rev. Lett.* **63** (1989) 2787.

[4] Particle Data Group, *Phys. Rev.* **D 50** (1994) 1173.

[5] OPAL Collaboration, P. D. Acton et al., *Phys. Lett.* **B 281** (1992) 405.

[6] ALEPH Collaboration, D. Buskulic et al., *Phys. Lett.* **B 297** (1992) 459.

[7] P. Overmann, 'A new method to measure the tau polarization at the Z peak', *Univ. of Dortmund: DO-TH* **93-24**, (1993).

[8] W. Bernreuther, O. Nachtmann, P. Overmann, *Phys. Rev.* **D 48** (1993) 78.

[9] OPAL Collaboration, K. Ahmet et al., *Nucl. Inst. and Meth.* **A 305** (1991) 275.

[10] P. P. Allport et al., *Nucl. Inst. and Meth.* **A 324** (1993) 34.

[11] OPAL Collaboration, R. Akers et al., *Phys. Lett.* **B 328** (1994) 207.

[12] P. E. Condon, P. L. Cowell, *Phys. Rev.* **D9** (1974) 2558.

[13] S. Jadach, B. F. L. Ward, Z. Wąs, *Comp. Phys. Comm.* **66** (1991) 276.

[14] S. Jadach, J. H. Kühn, Z. Wąs, *Comp. Phys. Comm.* **64** (1991) 275.

[15] J. Allison et al., *Nucl. Inst. and Meth.* **A 317** (1992) 47.

[16] J. Allison et al., *Comp. Phys. Comm.* **47** (1987) 55.

[17] P. Overmann, Fachbereich Physik, Univ. of Dortmund, private communication.

[18] J. H. Kühn, 'Tau kinematics from impact parameters', *Inst. f. theor. Teilchenphys., Univ. Karlsruhe*, preprint: TTP **93-14** (1993).

[19] Y. S. Tsai, *Phys. Rev.* **D 4** (1971) 2821.

[20] M. Davier, L. Duflot, F. Le Diberder, A. Rougé, *Phys. Lett.* **B 306** (1993) 411.